Experimental Investigation and Thermodynamic Modeling of the B_2O_3-FeO-Fe_2O_3-Nd_2O_3 System for Recycling of NdFeB Magnet Scrap

LARS KLEMET JAKOBSSON, GABRIELLA TRANELL, and IN-HO JUNG

NdFeB magnet scrap is an alternative source of neodymium that could have a significantly lower impact on the environment than current mining and extraction processes. Neodymium can be readily oxidized in the presence of oxygen, which makes it easy to recover neodymium in oxide form. Thermochemical data and phase diagrams for neodymium oxide containing systems is, however, very limited. Thermodynamic modeling of the B_2O_3-FeO-Fe_2O_3-Nd_2O_3 system was hence performed to obtain accurate phase diagrams and thermochemical properties of the system. Key phase diagram experiments were also carried out for the FeO-Nd_2O_3 system in saturation with iron to improve the accuracy of the present modeling. The modified quasichemical model was used to describe the Gibbs energy of the liquid oxide phase. The Gibbs energy functions of the liquid phase and the solids were optimized to reproduce all available and reliable phase diagram data, and thermochemical properties of the system. Finally the optimized database was applied to calculate conditions for selective oxidation of neodymium from NdFeB magnet waste.

DOI: 10.1007/s11663-016-0748-0

I. INTRODUCTION

THE transition from fossil fuels to renewable energy sources is creating an increasing demand for highly efficient electrical engines and electrical generators. One of the core components of these engines is NdFeB magnets, and hence the demand for neodymium is increasing rapidly. Neodymium like all other rare earth elements is mainly present in low-grade ores in a limited number of geographic locations. This has caused concerns over the supply of neodymium. The nature of these ores (low grade, often containing radioactive isotopes) makes mining and extraction of neodymium a high environmental impact operation.

Recycling of neodymium from NdFeB magnet containing waste is an attractive alternative to reduce the supply concern and environmental impact of neodymium production. Neodymium, however, reacts with oxygen to form one of the most stable oxides that exist, which makes it very hard to recover neodymium in metallic form. Understanding the oxidation of NdFeB magnets would make it easier to make a process for recovery of neodymium. Thermochemical and phase diagram data are essential for this understanding, but presently such data are very limited for the iron-saturated FeO-B_2O_3-Nd_2O_3 system.

The present work was conducted to find a self-consistent dataset for the iron-saturated FeO-B_2O_3-Nd_2O_3 system. The modified quasichemical model (MQM)[1] was used for the liquid solution while all ternary compounds were assumed to be stoichiometric. All relevant literature was critically reviewed, and optimization of all relevant systems was carried out. In addition, key phase diagram experiments were conducted to prepare the final thermodynamic description of the iron-saturated FeO-B_2O_3-Nd_2O_3 system. Fe_2O_3 also had to be included in the model to account for varying oxidation state of iron. Therefore, thermodynamic modeling of the entire B_2O_3-FeO-Fe_2O_3-Nd_2O_3 system was conducted.

II. THERMODYNAMIC MODELING

A. *Stoichiometric Compounds*

The Gibbs energy of a stoichiometric compound (solid and liquid) or gas can be expressed by:

$$G_T^{\circ} = H_T^{\circ} - TS_T^{\circ}, \quad [1]$$

$$H_T^{\circ} = \Delta H_{298K}^{\circ} + \int_{298K}^{T} C_p \, dT, \quad [2]$$

$$S_T^{\circ} = S_{298K}^{\circ} + \int_{298K}^{T} \left(C_p/T\right) dT, \quad [3]$$

LARS KLEMET JAKOBSSON, formerly Postdoctoral Fellow with NTNU Norwegian University of Science and Technology, Høgskoleringen 1, NO-7491 Trondheim, Norway, is now R&D Engineer with Elkem Technology, Fiskaaveien 100, NO-4675 Kristiansand, Norway. Contact e-mail: lars.k.jakobsson@elkem.com GABRIELLA TRANELL, Professor, is with NTNU Norwegian University of Science and Technology, Høgskoleringen 1, 7491 Trondheim, Norway. IN-HO JUNG, Professor, is with McGill University, 3610 University, H3A 0C5, Montreal, QC, Canada.
Manuscript submitted February 10, 2016.
Article published online July 21, 2016.

where ΔH^{o}_{298K} is the standard enthalpy of formation of a given compound at 298 K (25 °C). ΔH^{o}_{298K} of elemental species stable at 298 K (25 °C) and 1 atm is assumed to be 0 J mol^{-1} as a reference. S^{o}_{298K} is the standard entropy at 298 K (25 °C) and C_p is the heat capacity of a compound.

The Gibbs energies of the solid and liquid of FeO, Fe_2O_3, B_2O_3, Nd_2O_3, and other gas species needed for the present modeling were taken from the FactSage pure substance database.[2]

B. *Liquid Solution*

The MQM,[1] which takes into account short-range ordering of the second-nearest neighbors of cations with O^{2-} as a common anion in the oxide melt, was used for describing the slag. A brief description of the MQM is given below. In the MQM, the quasichemical reaction between A and B is described as

$$(A\text{–}A) + (B\text{–}B) = 2(A\text{–}B); \Delta g_{AB}, \quad [4]$$

where A and B are cations in liquid slag like Fe^{2+}, Fe^{3+}, Nd^{3+}, and B^{3+}, and $(i - j)$ represents an $i - j$ pair which is the second-nearest neighbor pair with common oxygen anion. Δg_{AB} is the Gibbs energy of the pair-exchange reaction which can be expanded as a function of composition and temperature.

The Gibbs energy of a binary solution, G^m, can be expressed by:

$$G^m = \left(n_A g^{o}_A + n_B g^{o}_B\right) - T\Delta S^{config} + \left(\frac{n_{AB}}{2}\right)\Delta g_{AB}, \quad [5]$$

where n_i and g^{o}_i are the number of moles and the molar Gibbs energy of the pure component i, and n_{AB} represents the number of moles of the (A–B) pair at equilibrium. ΔS^{config} is the configurational entropy of mixing, which is given by randomly distributing the (A–A), (B–B), and (A–B) pairs:

$$\Delta S^{config} = -R(n_A \ln X_A + n_B \ln X_B) - R\left[n_{AA}\ln\left(\frac{X_{AA}}{Y_A^2}\right) + n_{BB}\ln\left(\frac{X_{BB}}{Y_B^2}\right) + n_{AB}\ln\left(\frac{X_{AB}}{2Y_A Y_B}\right)\right], \quad [6]$$

where R is gas constant, n_i and X_i are the number of mole and mole fraction of component i in solution, respectively. n_{ij} and X_{ij} are the number of mole and pair fraction of (i–j) pair, respectively, and Y_i is an equivalent fraction of component i:

$$X_{ij} = n_{ij}/(n_{AB} + n_{AA} + n_{BB}), \quad [7]$$

$$Y_A = Z_A n_A/(Z_A n_A + Z_B n_B) = 1 - Y_B = X_{AA} + X_{AB}/2, \quad [8]$$

where the coordination numbers, Z_i, are defined by the following relationships:

$$Z_A n_A = 2n_{AA} + n_{AB}, \quad [9]$$

$$Z_B n_B = 2n_{BB} + n_{AB}. \quad [10]$$

The coordination numbers of Fe^{2+} and Fe^{3+} are 1.37744375 and 2.06616563, respectively, as in the current FactSage FToxid database.[2] The coordination numbers of B^{3+} and Nd^{3+} are set to be the same as that of Fe^{3+} in the present study. The Gibbs energy of a pair-exchange reaction, Δg_{AB}, is expanded in terms of the pair fractions, X_{ij}:

$$\Delta g_{AB} = \Delta g^{0}_{AB} + \sum_{i\geq 1} g^{i0}_{AB} X^{i}_{AA} + \sum_{j\geq 1} g^{0j}_{AB} X^{j}_{BB}, \quad [11]$$

where Δg^{0}_{AB}, g^{i0}_{AB}, and g^{0j}_{AB} are the model parameters which may be functions of temperature. These parameters can be optimized to reproduce the thermodynamic properties of the liquid phase and phase diagram data.

In the present study, the model parameters Δg_{AB} of binary B_2O_3-FeO, B_2O_3-Fe_2O_3, B_2O_3-Nd_2O_3, FeO-Nd_2O_3, and Fe_2O_3-Nd_2O_3 melts were optimized based on the available experimental data. Once the binary Δg_{AB} parameters are optimized the Gibbs energy of liquid solutions of ternary, and higher order systems can be predicted using the geometric extrapolation technique developed by Pelton.[3] In the present study, the Gibbs energies of all ternary liquid solutions of the B_2O_3-FeO-Fe_2O_3-Nd_2O_3 system were predicted using the Kohler interpolation technique.

III. CRITICAL EVALUATIONS, KEY PHASE DIAGRAM EXPERIMENTS, AND THERMODYNAMIC OPTIMIZATIONS

There is no complete experimental investigation of the B_2O_3-FeO-Fe_2O_3-Nd_2O_3 system. Only some thermochemical and phase diagram data for the subsystems are available. Thermodynamic optimization (modeling) of the FeO-Fe_2O_3 system is available in the FactSage FToxid database.[2] No modeling of other binary systems or higher order systems of the B_2O_3-FeO-Fe_2O_3-Nd_2O_3 system are available in literature. A critical evaluation experimental data was therefore performed and used to make a thermodynamically optimized model. Key phase diagram experiments were also done where data were missing. All the optimized model parameters in the present study are available in Table I.

A. *The Binary B_2O_3-Nd_2O_3 System*

1. *Literature review*

The binary B_2O_3-Nd_2O_3 system has been investigated in several works.[4–8] Three stable compounds are known in this system: $NdBO_3$,[4] NdB_3O_6,[5] and

Table I. Optimized Model Parameters for the B_2O_3-FeO-Fe_2O_3-Nd_2O_3 System. The B_2O_3-Fe_2O_3 system was modeled as an ideal liquid solution

Phase	Thermodynamic Parameters (J mol^{-1} or J mol^{-1} K^{-1})
Liquid	$\Delta g_{Fe^{2+}B^{3+}} = -29,288 + 8.368T + 35,564X_{Fe^{2+}Fe^{2+}} + 62764X^3_{Fe^{2+}Fe^{2+}} + (9205 + 8.368T)X_{B^{3+}B^{3+}} + (58,576 + 33.472T)X^6_{B^{3+}B^{3+}}$ $\Delta g_{Nd^{3+}B^{3+}} = -101,002 + 27.614T - 31,380X_{Nd^{3+}Nd^{3+}} + 18,200X_{B^{3+}B^{3+}} 20,920X^3_{B^{3+}B^{3+}} + 3766X^5_{B^{3+}B^{3+}}$ $\Delta g_{Fe^{3+}Nd^{3+}} = -38,723 J/mol$ $\Delta g_{Fe^{2+}Nd^{3+}} = -1966 J/mol$
$NdBO_3$ 298 ≤ T ≤ 1191.5 K (25 ≤ T ≤ 918.35 °C) 1191.5 ≤ T ≤ 1395 K (918.35 ≤ T ≤ 1121.85 °C) 1395 ≤ T ≤ 3000 K (1121.85 ≤ T ≤ 2726.85 °C)	$\Delta H_{298K} = -1,610,910, S_{298K} = 106.262$ $C_p = 151.295 + 0.018122T - 228,642T^{-2} - 1159.824T^{-0.5}$ $C_p = 121.652 + 0.015008T - 584,086T^{-2}$ $C_p = 141.712$
NdB_3O_6 298 ≤ T ≤ 1191.5 K (25 ≤ T ≤ 918.35 °C) 1191.5 ≤ T ≤ 1395 K (918.35 ≤ T ≤ 1121.85 °C) 1395 ≤ T ≤ 3000 K (1121.85 ≤ T ≤ 2726.85 °C)	$\Delta H_{298K} = -2,911,600, S_{298K} = 160.212$ $C_p = 338.361 + 0.024351T - 482,245T^{-2} - 3479.473T^{-0.5}$ $C_p = 249.431 + 0.015008T - 584,086T^{-2}$ $C_p = 269.491$
$Nd_4B_2O_9$ 298 ≤ T ≤ 1191.5 K (25 ≤ T ≤ 918.35 °C) 1191.5 ≤ T ≤ 1395 K (918.35 ≤ T ≤ 1121.85 °C) 1395 ≤ T ≤ 3000 K (1121.85 ≤ T ≤ 2726.85 °C)	$\Delta H_{298K} = -5043750, S_{298K} = 371.098$ $C_p = 418.115 + 0.066261T - 1,625,458T^{-2} - 2319.648T^{-0.5}$ $C_p = 358.828 + 0.060032T - 2,336,346T^{-2}$ $C_p = 439.069$
$NdFeO_3$ 298 ≤ T ≤ 2069 K (25 ≤ T ≤ 1795.85 °C) 2069 ≤ T ≤ 3000 K (1795.85 ≤ T ≤ 2726.85 °C)	$\Delta H_{298K} = -1,362,500, S_{298K} = 123.9$ $C_p = 146 + 0.00023T - 3,000,000T^{-2}$ $C_p = 145.77501$
FeB_4O_7 298 ≤ T ≤ 723 K (25 ≤ T ≤ 449.85 °C) 723 ≤ T ≤ 1644 K (449.85 ≤ T ≤ 1370.85 °C) 1644 ≤ T ≤ 3000 K (1370.85 ≤ T ≤ 2726.85 °C)	$\Delta H_{298K} = -2,843,350, S_{298K} = 167.396$ $C_p = 374.836 + 0.030608T - 2,533,300T^{-2} - 3353.051T^{-0.5} + 358,177,579T^{-3}$ $C_p = 241.384 + 0.030608T - 2,533,300T^{-2} + 1500.900T^{-0.5}$ $C_p = 327.607$

Table I. continued

Phase	Thermodynamic Parameters (J mol^{-1} or J mol^{-1} K^{-1})
$Fe_2B_2O_5$	$\Delta H_{298K} = -1,845,400, S_{298K} = 172.942$
$298 \le T \le 723$ K	$C_p = 160.381 + 0.061216T - 5,066,600T^{-2} + 574.825T^{-0.5} + 179,088,790T^{-3}$
$(25 \le T \le 449.85$ °C)	
$723 \le T \le 1644$ K	$C_p = 93.655 + 0.061216T - 5,066,600T^{-2} + 3001.8T^{-0.5}$
$(449.85 \le T \le 1370.85$ °C)	
$1644 \le T \le 3000$ K	$C_p = 266.102$
$(1370.85 \le T \le 2726.85$ °C)	
Fe_3BO_5	$\Delta H_{298K} = -1,630,400, S_{298K} = 198.934$
$298 \le T \le 723$ K	$C_p = 130.671 + 0.061216T - 6,520,420T^{-2} + 1788.312T^{-0.5} + 89,544,395T^{-3}$
$(25 \le T \le 449.85$ °C)	
$723 \le T \le 1644$ K	$C_p = 97.308 + 0.061216T - 6,520,420T^{-2} + 3001.8T^{-0.5}$
$(449.85 \le T \le 1370.85$ °C)	
$1644 \le T \le 3000$ K	$C_p = 269.755 - 1,453,820T^{-2}$
$(1370.85 \le T \le 2726.85$ °C)	

$Nd_4B_2O_9$.[7] The melting point of all these compounds have been determined in the previous works. The melting point of $NdBO_3$ was revised several times from the first measurement by Levin *et al.*[4] through the work by Roth *et al.*[9] to the final estimate of 1885 K ± 5 K (1612 °C) by Levin.[6] All these measurements were performed using the quenching method (QM). The melting point of NdB_3O_6 was determined to be 1428 K ± 5 K (1155 °C) by the same method in the work by Levin.[6] The melting point of $Nd_4B_2O_9$ was measured by Ji *et al.*[7] using differential thermal analysis (DTA) and found to be 1568 K ± 5 K (1295 °C).

$NdBO_3$ has a eutectic reaction with NdB_3O_6 where the eutectic temperature was found to be 1416 K (1143 °C) by Levin[6] and 1423 K ± 2 K (1150 °C) by Goryunova.[8] NdB_3O_6 has a monotectic reaction with liquid B_2O_3 at 1421 K ± 5 K (1148 °C) according to Levin *et al.*[5] and 1427 K ± 1 K (1154 °C) according to Goryunova.[8] Levin *et al.* used the QM for all their measurements while Goryunova used DTA. Ji *et al.*[7] found $Nd_4B_2O_9$ to react eutectically with Nd_2O_3 and $NdBO_3$ where the eutectic temperatures were found by DTA to be 1508 K ± 5 K (1235 °C) and 1483 K ± 5 K (1210 °C), respectively.

There are no studies on the thermal properties of $Nd_4B_2O_9$. Ji and Xi[10] have investigated $NdBO_3$ and NdB_3O_6. In this study, they determined the Gibbs energies of NdOF, $NdBO_3$, and NdB_3O_6 using electromotive force (EMF) measurements. One separate EMF measurement cell was used to determine the Gibbs energy of NdOF, while two EMF cells were used to determine the Gibbs energies of $NdBO_3$ and NdB_3O_6 simultaneously. Each cell configuration was as follows: Cell-1 "O_2, MgO + MgF_2//CaF_2//NdOF + Nd_2O_3, O_2", Cell-2 "O_2, MgO + MgF_2//CaF_2/ NdOF + $NdBO_3$ + NdB_3O_6, O_2", and Cell-3 "Cr + Cr_2O_2// ZrO_2//$NdBO_3$ + NdB_3O_6 + B." It should be noted that cell-2 was incorrectly written in the original manuscript of Ji and Xi (Nd_2O_3 was listed instead of $NdBO_3$), but according to their discussion in the manuscript, the cell configuration should be as described above. The measured Gibbs energy for NdOF from the first cell was used for determination of the Gibbs energies of $NdBO_3$ and NdB_3O_6.

2. *Optimization*

The Gibbs energies of $NdBO_3$ and NdB_3O_6 derived by Ji and Xi[10] were initially tested for the thermodynamic assessment, but it was impossible to reproduce the phase diagram using these values. The main problem was that the entropy of formation reported by Ji and Xi was too large. In addition, the Gibbs energy they used for Cr_2O_3 is different from the current literature value.[11] A closer examination of the work by Ji and Xi also revealed that the expression for the EMF for the third cell is slightly off-set from their measured values. The revised expression of their cell voltage should be

$$E_3 = 882 - 0.460\,T \quad (\text{mV}). \qquad [12]$$

Ji and Xi[10] did not investigate the chemical stability of their cells after the experiments. Careful examination of the EMF cell configurations of Ji and Xi showed that their EMF "Cell-3" may be thermodynamically unstable for determination of the targeted cell reaction. A recent assessment of the neodymium-boron system by Van Ende and Jung[12] was combined with the Gibbs energies measured by Ji and Xi for $NdBO_3$ and NdB_3O_6. The calculated equilibria showed that $NdBO_3$ and NdB_3O_6 are stable in equilibrium with NdB_6 in the temperature range where Ji and Xi investigated the Gibbs energy, instead of pure boron as assumed by them. This means that there is a very high probability that the EMF measurements were not performed as they originally designed them. Considering that NdB_6 is the stable phase instead of B, their cell reactions were in the present study re-evaluated as

$$7Cr_2O_3(s) + 3NdBO_3(s) + 2NdB_6 = 14Cr(s) + 5NdB_3O_6(s). \quad [13]$$

To keep the internal consistency of the FactSage database, the Gibbs energy of NdB_6 was taken from Van Ende and Jung,[12] and the Gibbs energy of Cr_2O_3 was taken from Degterov and Pelton.[11] The resulting Gibbs energies of formation of $NdBO_3$ and NdB_3O_6 from pure Nd_2O_3(s) and B_2O_3(l) were found to be

$$\Delta G^{o}_{NdBO_3} = -85.5 + 0.0195\,T \quad (kJ/mol), \quad [14]$$

$$\Delta G^{o}_{NdB_3O_6} = -143.1 + 0.0586\,T \quad (kJ/mol). \quad [15]$$

These Gibbs energies are more negative than those originally estimated by Ji and Xi.[10] It should be noted that these evaluations are only based on the thermodynamic reactions. For the real cell reactions, however, kinetics is involved—hence it is not possible to make sure that these revised reactions occurred in their actual experiments. Therefore, even these revised data were not highly weighted in the present optimization.

In the present optimization, the liquid parameter, $\Delta g_{Nd^{3+}B^{3+}}$, was roughly optimized first based on the liquidus of Nd_2O_3 and the miscibility gap in the B_2O_3-rich region. The Gibbs energies of solid stoichiometric compounds were subsequently optimized to roughly reproduce the re-evaluated Gibbs energies of compounds from the EMF data by Ji and Xi[10] and the phase diagram. The entropies of all stoichiometric compounds in the B_2O_3-Nd_2O_3 system were estimated using the Neumann–Kopp rule. This rule was also applied to estimate the heat capacity of the compounds since there are no heat capacity data available for any of them. Then, the value of ΔH^{o}_{298K} for $NdBO_3$ was adjusted to reproduce the phase diagram. Iterative adjustments of $\Delta g_{Nd^{3+}B^{3+}}$ and ΔH^{o}_{298K} of compounds were done until the phase diagram was reproduced within the experimental uncertainty.

The optimized phase diagram from the present study is plotted in Figure 1 along with experimental data by Levin,[6] Ji *et al.*,[7] and Goryunova.[8] The optimized congruent melting temperature of $NdBO_3$ is 1885 K (1612 °C), matching the experimentally measured temperature by Levin *et al.*[6] The eutectic temperature between $NdBO_3$ and NdB_3O_6 was adjusted to be 1419 K (1146 °C), which is between the values found by Levin *et al.*[6] and Goryunova[8]. The same was done for the monotectic temperature, which was adjusted to 1423 K (1150 °C). This gave a melting point of NdB_3O_6 of 1423.5 K (1150.5 °C), which is a bit lower than the value of 1428 K (1155 °C) found by Levin *et al.*[6] The critical point of the miscibility gap has not been measured, and a tentative value of 1873 K (1600 °C) was set in the present optimization. The eutectic temperature between Nd_2O_3 and $Nd_4B_2O_9$ was adjusted to the value from Ji *et al.*[7] of 1508 K (1235 °C). The eutectic between $Nd_4B_2O_9$ and $NdBO_3$ from the optimized model was 1487 K (1214 °C), which is slightly higher than the value from Ji *et al.* of 1483 K (1210 °C). Finally, the melting point of $Nd_4B_2O_9$ from the optimization was 1519 K (1246 °C), which is significantly lower than the melting point of 1568 K (1295 °C) found by Ji *et al.*

The optimized Gibbs energies of formations of the stoichiometric $NdBO_3$ and NdB_3O_6 compounds from Nd_2O_3(s) and B_2O_3(l) are plotted in Figure 2. The original data from Ji and Xi[10] and the revised data from the present study are compared with the optimized results. The best reproduction of the phase diagram was achieved with a somewhat more negative Gibbs energy of $NdBO_3$ than the revised data from Ji and Xi at 1172 K (899 °C) (−62.6 *vs* −51.9 kJ mol^{-1}). For NdB_3O_6, the Gibbs energy in the present work was calculated to be almost half of the value measured by Ji and Xi[10] at 1172 K (899 °C) (−74.6 *vs* −122.9 kJ mol^{-1}). As shown in the phase diagram in Figure 1, $NdBO_3$ has the most stable congruent melting temperature. This means that most probably the Gibbs energy of formation of $NdBO_3$ in one mole of the Nd_2O_3-B_2O_3 system should have the lowest value. However, according to the experimental data by Ji and Xi, the gram mole Gibbs energy of formation of NdB_3O_6 has lower value than $NdBO_3$, which is highly unrealistic and could not reproduce the phase diagram data at all.

B. *The FeO-B_2O_3 System*

1. *Literature review*

Very limited experimental data are available in the iron-saturated FeO-B_2O_3 system. One unpublished study by Kosh *et al.* is cited in the Slag Atlas.[13] In their study, the compound $Fe_3B_2O_6$ was indicated but it is not documented anywhere else. The compound FeB_2O_4 has been reported only as a high-pressure phase.[14,15] Block *et al.*[16] and Kawano *et al.*[17] reported the last compound indicated by Kosh *et al.* $Fe_2B_2O_5$, to be stable at standard atmospheric pressure. From the single crystal growth experiments by Kawano *et al.*, it would be expected that the melting point of $Fe_2B_2O_5$ is between 1223 K and 1273 K (950°C and 1000 °C).

Kawano *et al.*[17] also observed that Fe_3BO_5 formed when they were on the FeO-rich side of $Fe_2B_2O_5$. It should be noted that Fe_3BO_5 also contains iron in the

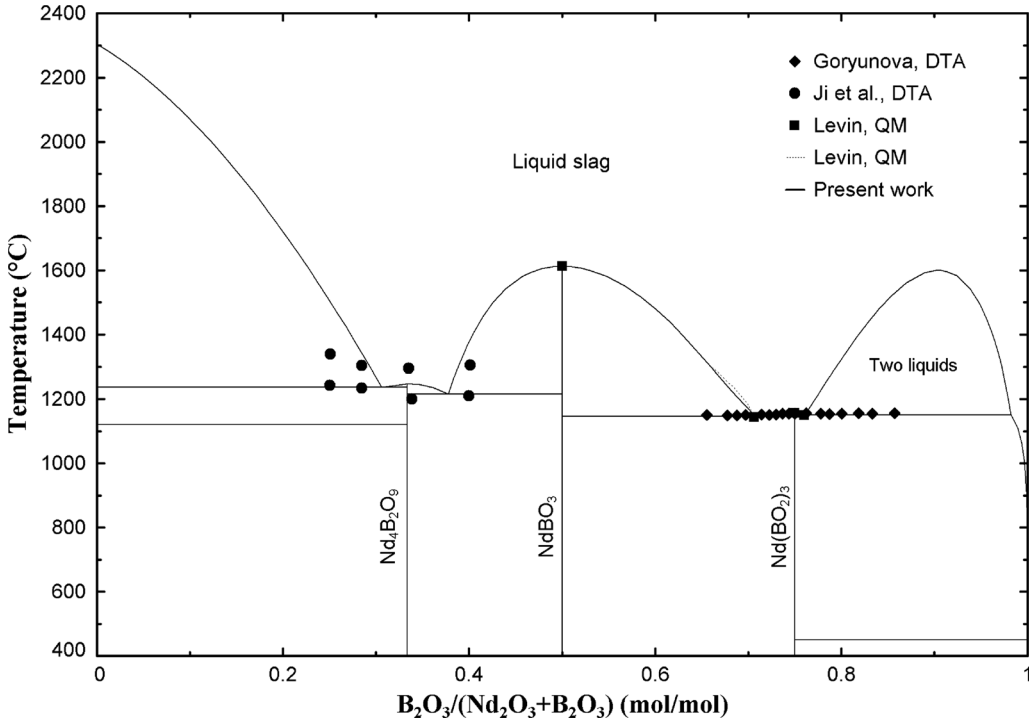

Fig. 1—The optimized phase diagram of the B_2O_3-Nd_2O_3 system along with experimental data.[6–8]

3+ oxidation state. Kravchuk and Lazebnik[18] also observed Fe_3BO_5 in equilibrium with $Fe_2B_2O_5$ and iron. Kosh *et al.* did not indicate the compound FeB_4O_7 in their study, but it has been documented by Kravchuk and Lazebnik,[18] and Rumanova *et al.*[19] Kravchuk and Lazebnik obtained single crystals of FeB_4O_7 at 973 K (700 °C), and found it to be stable in the whole range from 523 K to 973 K (250 °C to 700 °C).

Dong *et al.*[20] studied the solid-phase equilibria at 903 K (630 °C) under 95 pct argon + 5 pct hydrogen atmosphere and found FeB_4O_7, FeB_2O_4, and Fe_3BO_5 to be the only existing phases by XRD. These results suggests that FeB_2O_4 may exist as a stable phase even at atmospheric pressure and that $Fe_2B_2O_5$ may not be stable at lower temperatures. Further studies should be conducted to investigate this, and these results were not used in the present study.

Only one study was found on the thermodynamic properties in the FeO-B_2O_3 system Fujiwara *et al.*[21] used electrochemical cell measurements to determine the activities of FeO and B_2O_3 at 1473 K, 1573 K, and 1673 K (1200 °C, 1300 °C, and 1400 °C) under iron saturation. They also determined the positions of the liquidus line of FeO and the miscibility gap on the FeO-rich side at these temperatures.

2. *Optimization*

Figure 3 shows the optimized phase diagram of the iron-saturated FeO-B_2O_3 system. The liquid solution parameters of the iron-saturated FeO-B_2O_3 system were adjusted according to the activity measurements by Fujiwara *et al.*,[21] as shown in Figure 4. In addition, the phase boundaries found by Fujiwara *et al.* were used for the liquidus of FeO and miscibility gap in the B_2O_3-rich region. The heat capacities and entropies at 298 K (25 °C) of Fe_3BO_5, $Fe_2B_2O_5$, and FeB_4O_7 were estimated using the Neumann-Kopp rule due to lack of experimental data.

The enthalpy of formation of $Fe_2B_2O_5$ was adjusted to reproduce the expected melting point of approximately 1248 K (975 °C) from Kawano *et al.*[17] The enthalpy of formation of Fe_3BO_5 was adjusted to give a tentative melting point of 1373 K (1100 °C), which is low enough to keep $Fe_2B_2O_5$ as a congruently melting compound and high enough to keep Fe_3BO_5 and $Fe_2B_2O_5$ existing in equilibrium. Finally, the enthalpy of formation of FeB_4O_7 was adjusted to reproduce the stability up to 973 K (700 °C) found by Kravchuk and Lazebnik.[18]

The optimized phase diagram shows reasonable agreement with available data, but it should be noted that the available phase diagram data are very limited. It can be seen that the estimated diagram by Koch *et al.*[13] is quite different from the liquidus of FeO by Fujiwara *et al.*[21] In the present study, more weight was given to the data by Fujiwara *et al.* The experimental activity data of FeO are very well reproduced by the present optimization, as can be seen in Figure 4.

C. *The Fe_2O_3-B_2O_3 System*

No thermochemical data are reported in the Fe_2O_3-B_2O_3 system. Joubert *et al.*[22] investigated the stability of the two compounds Fe_3BO_6 and $FeBO_3$ in this system. This study was followed by a study by Makram *et al.*[23] where they investigated Fe_3BO_6 and

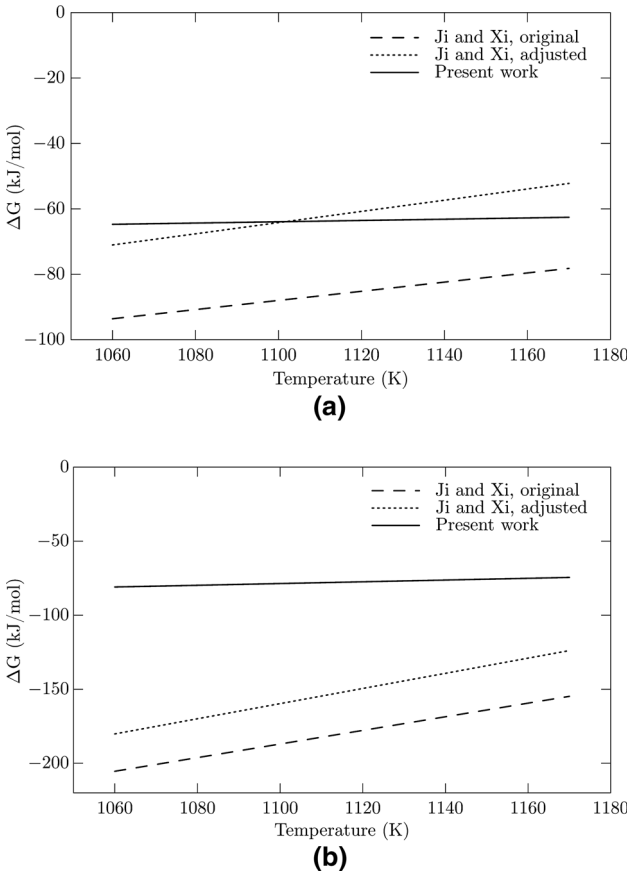

Fig. 2—The optimized Gibbs energies of formation of (*a*) $NdBO_3$ and (*b*) $Nd(BO_2)_3$ compounds in the B_2O_3-Nd_2O_3 system from Nd_2O_3(s) and B_2O_3(l), in comparison to original and revised values from Ji and Xi.[10]

$FeBO_3$ in the temperature range from 670 °C to 900 °C. They found the decomposition temperatures to be somewhat lower than found by Joubert *et al.* Selcuk[24] investigated the solid and liquid phase boundaries of the Fe_2O_3-B_2O_3 system and found different phase equilibria than in previous works. Instead of Fe_3BO_6 and $FeBO_3$, they found a new compound, $Fe_2B_4O_9$, that had not been previously documented. The phase diagram derived from their work is therefore significantly different from the ones proposed by Joubert *et al.* and Makram *et al.*

Due to the discrepant and limited phase diagram data and lack of thermodynamic properties of both the liquid phase and of compounds, it is hard to optimize the binary system. For the purpose of the present study, however, it is not important to achieve accurate modeling of this system. So, the Gibbs energy of the compounds was not evaluated and the liquid phase was assumed to be an ideal solution.

D. *The Fe_2O_3-Nd_2O_3 System*

1. *Literature review*

The phase equilibria of the Fe_2O_3-Nd_2O_3 system were first investigated by Katsura *et al.*,[25] and they found $NdFeO_3$ to be the only stable compound. Nielsen and Blank[26] determined the melting point of $NdFeO_3$ to be 2068 K ± 8 K (1795 °C) in air. That was the only melting point of this compound found in literature.

Katsura *et al.*[25] determined the Gibbs energy of $NdFeO_3$ using CO_2-H_2 gas equilibration and a solid electrolyte cell, which measured the oxygen partial pressure in the range from 1347 K to 1620 K (1200 °C to 1347 °C). In these experiments, they found $NdFeO_3$ to decompose to metallic iron and Nd_2O_3. This means that the three phase equilibrium of Fe + Nd_2O_3 + $NdFeO_3$ occurs in the range from 1347 K to 1620 K (1200 °C to 1347 °C), and no ferrous (Fe^{2+}) oxide is involved in this decomposition reaction even at reducing conditions in the presence of metallic iron. Based on the experimental findings they could draw the ternary section of the Fe-Fe_2O_3-Nd_2O_3 system at 1473 K (1200 °C).[27]

The thermal properties of $NdFeO_3$ at somewhat lower temperatures were recently investigated by Parida *et al.*[28] They used a Calvet microcaliometer to measure enthalpy increments from 299 K to 1000 K (26 °C to 727 °C). From 1004 K to 1208 K (731 °C to 935 °C), they used a reversible EMF cell to measure the Gibbs energy, and by linear extrapolation to higher temperatures, they found good agreement with the measurements by Katsura *et al.*[25] Vorobev *et al.*[29] reviewed available experimental literature where they included one dataset from Russian literature. These data also agree relatively well with the measurements by Katsura *et al.*[25] and Parida *et al.*[28]

2. *Optimization*

The calorimetry data by Parida *et al.*[28] were used for the heat capacity of $NdFeO_3$. The enthalpy and entropy of $NdFeO_3$ were also taken from the study by Parida *et al.* The Gibbs energy of $NdFeO_3$ used in the present study is presented in Figure 5 along with experimental data.

The model parameter of the liquid solution was optimized in order to reproduce the melting point of $NdFeO_3$ in air found by Nielsen and Blank[26] of 2068 K ± 8 K (1795 °C). Due to the lack of phase diagram data other than the melting temperature of $NdFeO_3$, a single parameter of $\Delta g^{o}_{Fe^{3+}Nd^{3+}}$ was optimized. The optimized phase diagram of the Fe_2O_3-Nd_2O_3 system in air is plotted in Figure 6. Two eutectic temperatures of $NdFeO_3$ + Fe_3O_4 → L and $NdFeO_3$ + Nd_2O_3 → L are predicted at 1697 K and 1945 K (1424 °C and 1672 °C), respectively.

E. *The FeO-Nd_2O_3 System*

1. *Key phase diagram experiments*

To the present authors' knowledge, no experimental phase diagram data are available for the iron-saturated FeO-Nd_2O_3 system. Therefore, key phase diagram experiments were performed in the present study using the classical quenching method (QM) and the differential thermal analysis (DTA) technique.

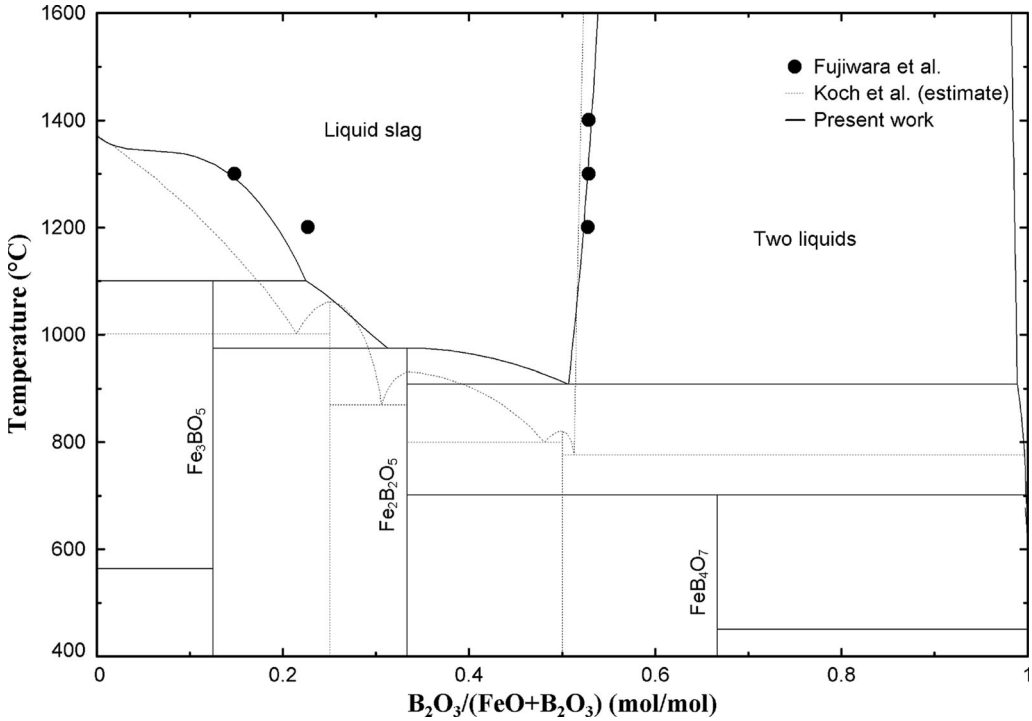

Fig. 3—Optimized phase diagram of the B_2O_3-FeO system saturated with iron along with experimental data from Fujiwara *et al.*[21] and estimated diagram by Koch *et al.*[13]

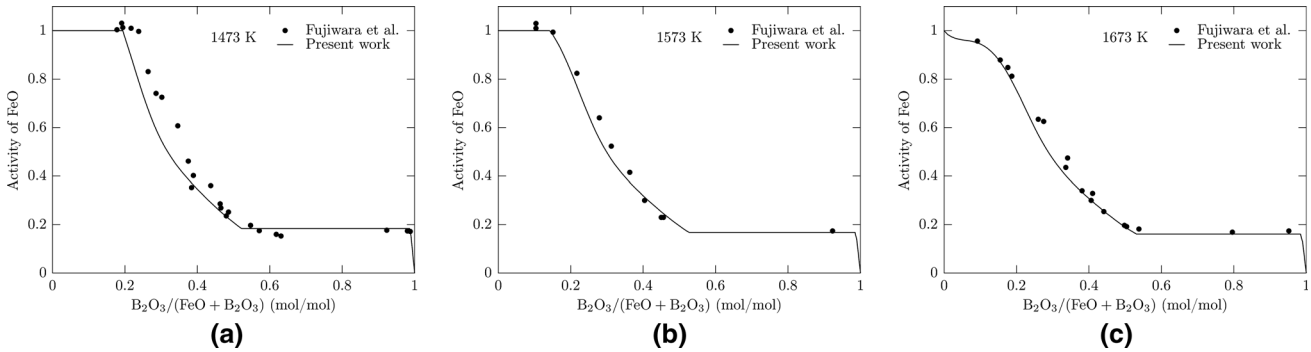

Fig. 4—Optimized activity of solid FeO (liquid FeO at 1623 K (1400 °C)) in the B_2O_3-FeO system saturated with iron compared with experimental data from Fujiwara *et al.*[21]

The reagent chemicals were powders of Fe_2O_3 (99.998 pct, Alfa Aesar), Nd_2O_3 (99.99 pct, Alfa Aesar), and iron (≥99.9 pct, Alfa Aesar). These powders were weighed and mixed to give the targeted compositions with 50 pct excess iron. The reagent chemicals and prepared mixtures were stored in a desiccator filled with silica gel due to the hygroscopic nature of the oxides and the corrosion potential of iron. The moisture content in the reagent Fe_2O_3 was found to be negligible by checking the mass loss (0.09 pct) of a control sample after heating to 398 K (125 °C) in air for 24 hours. The mass loss from the reagent Nd_2O_3 was found to be 0.23 pct after heating to 1273 K (1000 °C) for 3 hours in air. The mixing of reagents for the FeO-Nd_2O_3 mixtures was done for 15 minutes in an agate mortar under 99.9 pct isopropanol. Iron crucibles with outer diameter 6 mm,

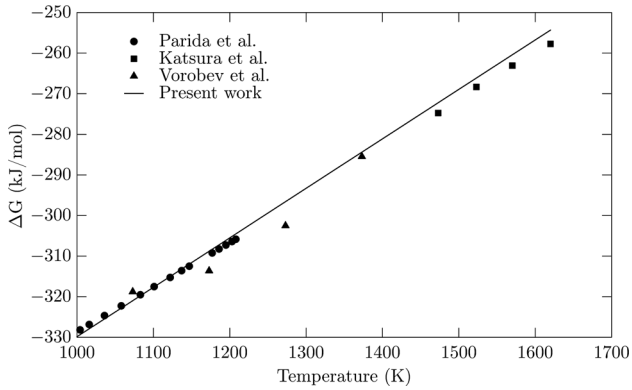

Fig. 5—Optimized Gibbs energy of $NdFeO_3$ from Nd_2O_3, iron, and O_2(g) along with experimental data.[25,28,29]

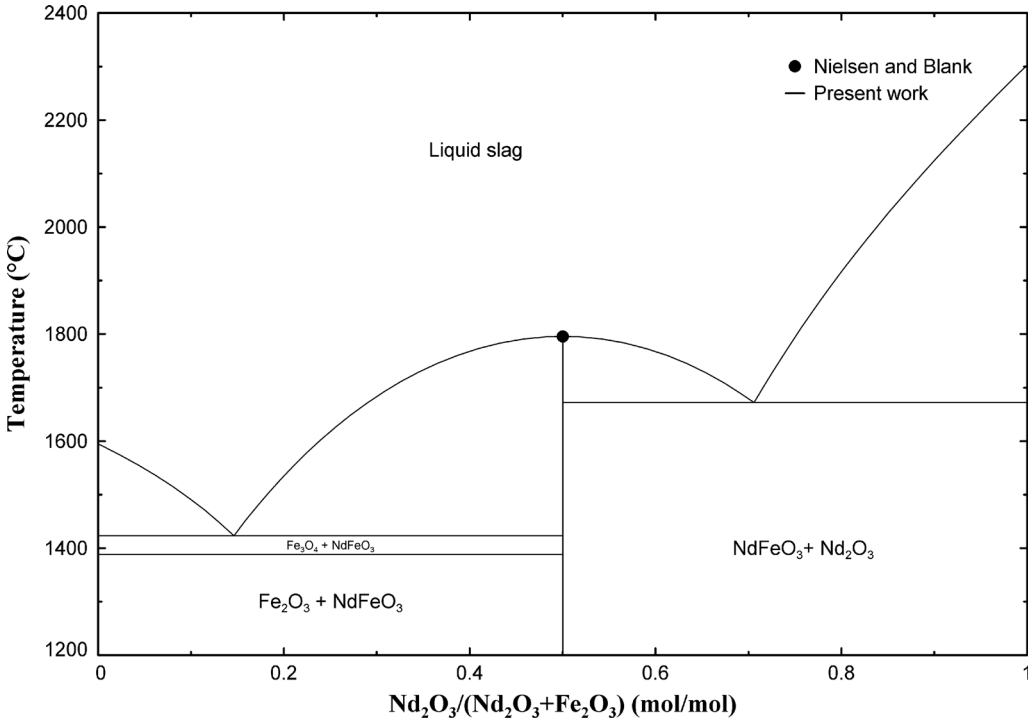

Fig. 6—Optimized phase diagram of the Fe_2O_3-Nd_2O_3 in air along with the experimentally measured melting temperature of $NdFeO_3$ from Nielsen and Blank.[26]

inner diameter 4 mm, and height 18–20 mm were made from a 99.5 pct pure iron tube (one end was sealed by welding). The tubes were filled with approximately 200 mg of material before they were clamped and welded to sealed capsules.

Three different compositions were prepared: 40FeO-60Nd_2O_3, 60FeO-40Nd_2O_3, and 95FeO-5Nd_2O_3 (compositions in mole percent). The classical quenching experiments were carried out using a vertical tube furnace. In order to prevent oxidation of the iron capsules during the experiment, high-purity Ar gas (6N) was purged into the tube during the experiments. The capsules containing all three compositions were held at 1473 K (1200 °C) for 18 hours. Two samples of 40FeO-60Nd_2O_3 and 60FeO-40Nd_2O_3 were also held at 1673 K (1400 °C) for 6 hours. After targeted equilibration time, the capsules were quenched by dropping directly from the hot zone into a container with water. The capsules were subsequently mounted in epoxy and polished for EPMA. Small amounts of sample were also extracted for XRD analysis.

Sealed iron crucibles containing samples were used for DTA as well. Approximately, 100 mg of mixed material was filled in each iron crucible. These crucibles were made from 99.85 pct pure iron and had the same dimensions as the capsules used for the quenching experiments except for a lower height of 12 mm and a flat bottom. The crucible containing samples was first held at 1273 K (1000 °C) for one hour under 6N argon atmosphere to remove any hydrocarbons, moisture, hydroxide, or carbonates that could have been introduced or formed during mixing. The mass loss was typically 1 mg or less. The opening was then clamped and the crucibles were welded to sealed capsules. The sealed capsules were held at 1723 K (1450 °C) for one hour under argon atmosphere for premelting and homogenization before cooling back to room temperature. Then, the capsules were investigated by DTA using a Netzsch STA 449C Jupiter, where they were held in an alumina cup. The temperature measurements of this apparatus were calibrated against the melting point of gold. The capsules were heated under 98 pct argon + 2 pct hydrogen by 10 K min^{-1} to 1723 K (1450 °C) and cooled by the same rate back to room temperature. Transition temperatures were determined as the extrapolated onset temperature of the exothermic and endothermic peaks. Eight different compositions in the iron-saturated FeO-Nd_2O_3 system were investigated by DTA.

2. *Experimental results and optimization*

The experimental results of quenching runs are summarized in Table II, and the results of DTA are summarized in Table III. The stoichiometry of phases after the quenching experiments were determined by EPMA and the phases were confirmed by XRD.

Figure 7 shows the microstructures of two quenched samples from the present study. The microstructure of the capsule containing 95FeO-5Nd_2O_3 after annealing at 1473 K (1200 °C) for 18 hours is shown in Figure 7(a). $NdFeO_3$ crystals are observed in equilibrium with FeO and iron. The capsules containing 40FeO-60Nd_2O_3 and 60FeO-40Nd_2O_3 still contained unreacted powders even after being held at 1473 K (1200 °C) for 18 hours. The capsules held at 1400 °C for 6 hours had $NdFeO_3$ in equilibrium with Nd_2O_3 and iron after quenching. The microstructure of the capsule containing

Table II. Quenching Experiments in the Iron-Saturated FeO-Nd_2O_3 System

Temperature, K (°C)	Composition (mol pct)		Phases After Equilibration			
	FeO	Nd_2O_3	FeO	Nd_2O_3	$NdFeO_3$	Fe
1673 (1400)	40	60	no	yes	yes	yes
1673 (1400)	60	40	no	yes	yes	yes
1473 (1200)	40	60		unreacted		
1473 (1200)	60	40		unreacted		
1473 (1200)	95	5	yes	no	yes	yes

Table III. Starting Compositions of Materials and Extrapolated Onset Temperatures from the DTA Experiments in the Iron-Saturated FeO-Nd_2O_3 System

Composition (mol pct)		Onset Temperature, K (°C)	
FeO	Nd_2O_3	Heating	Cooling
40	60	1595.0 (1321.8)	1606.3 (1333.1)
50	50	1604.8 (1331.6)	1610.9 (1337.7)
55	45	1593.7 (1320.5)	1611.4 (1338.2)
60	40	1605.6 (1332.4)	1609.3 (1336.1)*
75	25	1611.5 (1338.3)	1619.1 (1345.9)
85	15	1511.3 (1238.1)	1511.9 (1238.7)*
90	10	1512.7 (1239.5)	1511.2 (1238.0)
95	5	1509.9 (1236.7)	1511.3 (1238.1)**

* Heating and cooling rate of 3 K min^{-1} between 1423 K and 1723 K (1150 °C and 1450 °C).
** Heating and cooling rate of 1 K min^{-1} between 1473 K and 1673 K (1200 °C and 1400 °C).

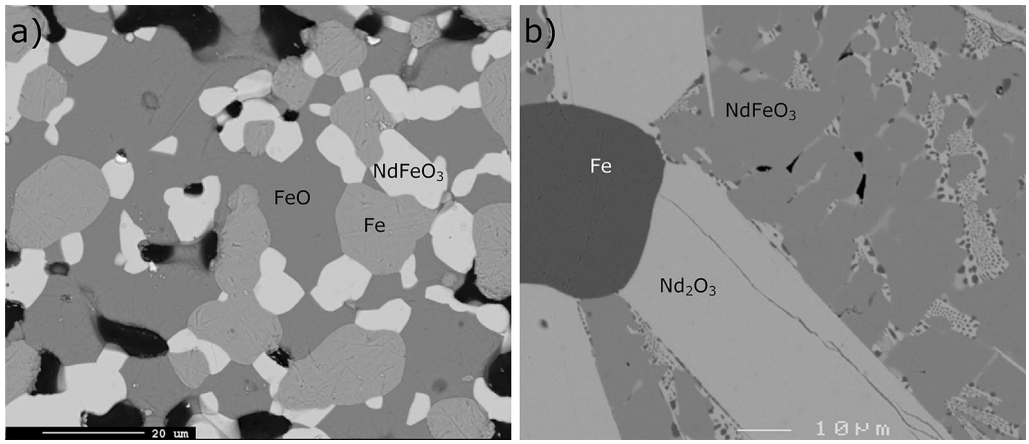

Fig. 7—Microstructure of samples after equilibration. (*a*) 95FeO-5Nd_2O_3 quenched from 1473 K (1200 °C). (*b*) 40FeO-60Nd_2O_3 quenched from 1673 K (1400 °C).

40FeO-60Nd_2O_3 is shown in Figure 7(b). Some regions where Nd_2O_3 and iron were intermixed were observed in between $NdFeO_3$ grains, as can be seen in Figure 7(b). This seems to happen due to the liquid phase decomposing to Nd_2O_3 and iron during cooling, as explained by the final optimized phase diagram of the Fe-Fe_2O_3-Nd_2O_3 system below. This also indicated that the quench was not rapid enough to form a glass from the liquid phase.

The optimized phase diagram of the iron-saturated FeO-Nd_2O_3 is calculated in Figure 8. As determined from the quenching experiment, there is only one intermediate phase in the FeO-Nd_2O_3-Fe system. Surprisingly, the intermediate phase is not in this section (no ferrous neodymium oxide phase exists), but $NdFeO_3$ where iron is in ferric state is existing here. That is, the '$NdFeO_3$ + Fe' mixture is the stable phase in this FeO-Nd_2O_3 section as calculated in Figure 9. This result is consistent with the previous study by Katsura *et al.*[25] who measured the Gibbs energy of $NdFeO_3$ from a Fe + Nd_2O_3 mixture, which also led them to report the diagram of the Fe-Nd_2O_3-Fe_2O_3 system in their later study.[27]

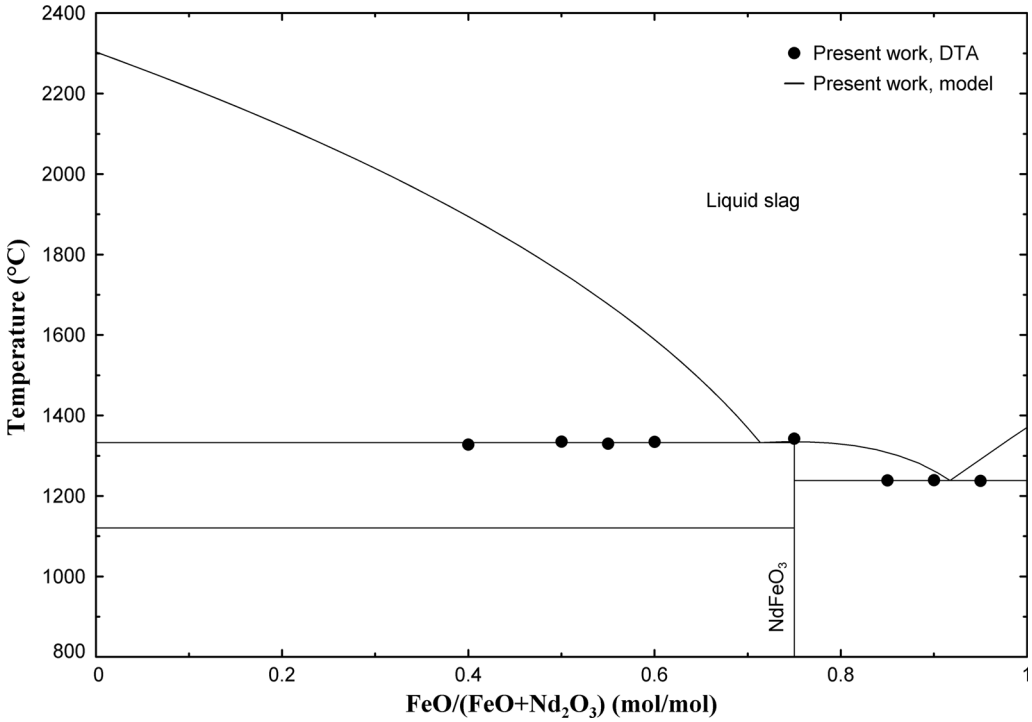

Fig. 8—The optimized phase diagram of the iron-saturated FeO-Nd_2O_3 system together with DTA measurements conducted in the present work.

The DTA results are also plotted in Figure 8. The extrapolated onset temperature during cooling is very close to the onset temperature during heating in the region between FeO and $NdFeO_3$. The eutectic temperature for FeO + $NdFeO_3 \rightarrow$ L was determined as the mean value of onset temperatures during heating and cooling. The mean temperature of all three compositions was 1511.4 K (1238.2 °C). For the compositions between Nd_2O_3 and $NdFeO_3$, the onset temperatures during cooling were higher than those during heating by 9.7 K on average. The reason for such discrepancy was not further investigated. In the present study, the average of heating and cooling was taken. The mean temperature of all four compositions was 1604.6 K (1331.5 °C). For the composition of 75FeO-25Nd_2O_3 (melting temperature of $NdFeO_3$), the mean transition temperature was 1615.3 K (1342.1 °C).

A small negative solution parameter was added to liquid FeO-Nd_2O_3 to adjust the phase diagram in accordance with the DTA measurements as shown in Figure 8. No adjustments were necessary apart from this to reproduce the phase diagram.

IV. APPLICATION TO RECYCLING PROCESSES

As mentioned earlier, there is no phase diagram or thermodynamic information for the FeO-Fe_2O_3-Nd_2O_3-B_2O_3 in oxidizing or reducing conditions. Therefore, the present optimization results were integrated with the previous results of FeO-Fe_2O_3 system in the FactSage FToxid database,[2] and a set of the oxide database was prepared. In the application calculations,

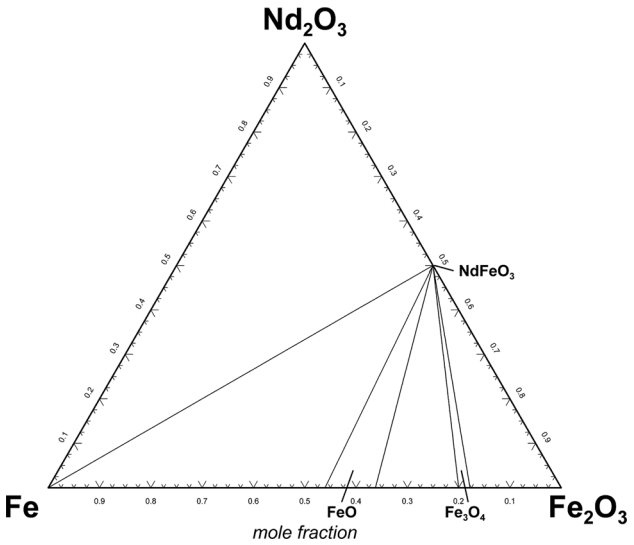

Fig. 9—Calculated ternary section of the Fe-Fe_2O_3-Nd_2O_3 system at 1473 K (1200 °C).

the previous database of the metallic Fe-Nd-B system optimized by Van Ende and Jung[12] and the FactSage pure substance database[2] were used together with the present database.

In order to investigate the selective oxidation process of NdFeB scrap into the B_2O_3-FeO-Fe_2O_3-Nd_2O_3 system, the phase stability diagram (partial pressure of oxygen *vs* temperature diagram) of $Nd_2Fe_{14}B$ magnets was calculated, as shown in Figure 10. According to the calculated results, molten slag with no remaining metal can be formed above 1673 K (1400 °C) and "oxidizing" conditions (log $PO_2 > -10$ atm). At somewhat lower

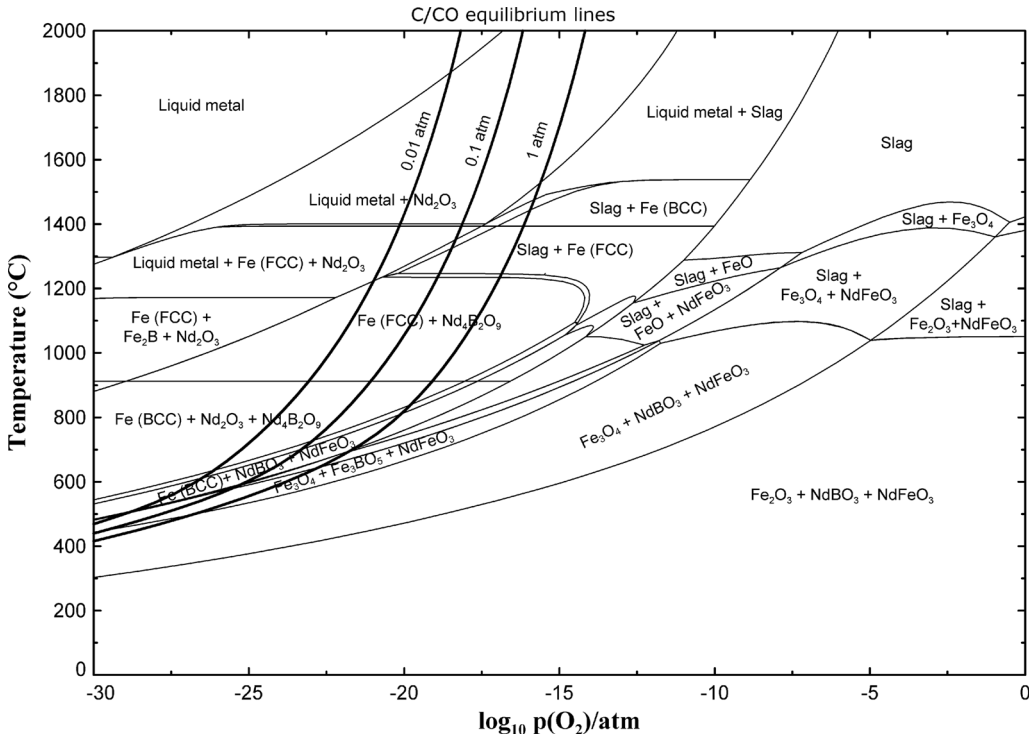

Fig. 10—Calculated phase stability diagram of a $Nd_2Fe_{14}B$ magnet depending on partial pressure of oxygen and temperature. Slag means molten oxide phase and liquid metal means liquid metallic solution.

partial pressures of oxygen, slag will be formed in equilibrium with metal. Under ''reducing'' conditions (log $PO_2 < -15$ atm), a metallic liquid Fe-B solution will be formed leaving Nd_2O_3 as a solid phase, as can be seen in the diagram. Once the partial pressure of oxygen is further reduced, no metal will be oxidized.

From a process design viewpoint, the metallic Fe-B liquid solution and solid Nd_2O_3 can be easily separated and high-purity Nd_2O_3 can be taken out from the system. If CO is used as an oxidizing agent, the C-CO equilibrium should be considered. The equilibrium partial pressures of oxygen developed by C–CO equilibration depending on temperature are superimposed in Figure 10. Solubility of carbon in the metallic phase and possible formation of (oxy)carbides was not considered. According to the diagram, NdFeB scrap can be selectively oxidized by CO with controlled pressure of 0.1 to 0.01 atm (diluted by inert gas or reduction of total gas pressure in reactor), and the mixture of 'liquid metal + Nd_2O_3' can be easily achieved.

V. SUMMARY

Critical evaluation and thermodynamic modeling of the B_2O_3-FeO-Fe_2O_3-Nd_2O_3 system was performed in this study. Key phase diagram experiments for the iron-saturated FeO-Nd_2O_3 system were also performed to assist the modeling. Thermodynamic modeling of the binary systems of B_2O_3-FeO, B_2O_3-Nd_2O_3, FeO-Nd_2O_3, and Fe_2O_3-Nd_2O_3 were performed. The liquid B_2O_3-Fe_2O_3 was assumed as an ideal solution due to limited available experimental data. The optimized model parameters were integrated to calculate the phase stability diagram of the NdFeB magnet depending on partial pressure of oxygen to provide a guidance for selective extraction of Nd_2O_3 during the recycling of the magnet scrap.

In order to improve the accuracy of the thermodynamic description, the phase diagram and thermodynamic properties of B_2O_3-Nd_2O_3, FeO-B_2O_3, and Fe_2O_3-B_2O_3 system should be further investigated. An investigation of the phase diagram of ternary or higher order systems would also be necessary.

ACKNOWLEDGMENT

This work was funded by research grant EU FP7-603564 – REEcover.

REFERENCES

1. A.D. Pelton, S.A. Degterov, G. Eriksson, C. Robelin, and Y. Dessureault: *Metall. Mater. Trans. B*, 2000, vol. 31B, pp. 651–59.
2. C.W. Bale, E. Bélisle, P. Chartrand, S.A. Decterov, G. Eriksson, K. Hack, I.-H. Jung, Y.B. Kang, J. Melançon, A.D. Pelton, and C. Robelin: *CALPHAD*, 2009, vol. 33 (2), pp. 295–311.
3. A.D. Pelton: *CALPHAD*, 2001, vol. 25 (2), pp. 319–28.
4. E.M. Levin, R.S. Roth, and J.B. Martin: *Am. Min.*, 1961, vol. 46, pp. 1030–55.
5. E.M. Levin: *Phys. Chem. Glasses*, 1966, vol. 7 (3), pp. 90–93.
6. E.M. Levin: in *Phase Diagrams: Materials Science and Technology, 1970-1978*, A.M. Alper, ed., Academic Press, New York, 1970, vol. 3, pp. 179–181.
7. Y. Ji, J. Liang, Z. Chen, and S. Xie: *J. Am. Ceram. Soc.*, 1991, vol. 74 (2), pp. 444–46.
8. A. Goryunova: Beitrag zur Kristallchemie und Kristallsynthese binärer Seltenerdborate vom Typ SEB_3O_6 und $SEBO_3$, Doctoral Dissertation, Universität zu Köln, 2003.
9. R.S. Roth, J.L. Waring, and E.M. Levin: *Proceedings of the 3rd Conference on Rare Earth Research*, Glenwood Springs, CO, Gordon and Breach, New York, 1963, pp. 153–63.
10. C. Ji and Z. Xi: *J. Less Common Met.*, 1990, vol. 158 (2), pp. 191–98.
11. S. Degterov and A.D. Pelton: *J. Phase Equilib.*, 1996, vol. 17 (6), pp. 476–87.
12. M.-A. Van Ende and I.-H. Jung: *J. Alloys Compd.*, 2013, vol. 548, pp. 133–54.
13. S. Atlas (ed): Verein Deutscher Eisenhuttenleute.Verlag Stahleisen mbH, FRG, Dusseldorf, 1981.
14. J.S. Knyrim and H. Huppertz: *J. Solid State Chem.*, 2008, vol. 181 (8), pp. 2092–98.
15. S.C. Neumair, R. Glaum, and H. Huppertz: *Zeitschrift für Naturforschung B*, 2009, vol. 64 (8), pp. 883–90.
16. S. Block, G. Burley, A. Perloff, and R.D. Mason, Jr: *J. Res. Natl. Bur. Stand.*, 1959, vol. 62, pp. 95–100.
17. T. Kawano, H. Morito, T. Yamada, T. Onuma, S.F. Chichibu, and H. Yamane: *J. Solid State Chem.*, 2009, vol. 182 (8), pp. 2004–09.
18. T.A. Kravchuk and Y.D. Lazebnik: *Russ. J. Inorg. Chem.*, 1967, vol. 12 (1), pp. 21–24.
19. T.M. Rumanova, E.A. Genkina, and N.V. Belov: *Izv. Akad. Nauk. Latv. SSR Ser. Khim.*, 1981, vol. 5, pp. 571–79.
20. Y.Z. Dong, Y.M. Zhao, P. Fu, H. Zhou, and X.M. Hou: *J. Alloys Compd.*, 2008, vol. 461 (1), pp. 585–90.
21. H. Fujiwara, H. Moriya, and M. Iwase: *Iron Steelmak*, 1991, vol. 18 (1), pp. 43–49.
22. J.C. Joubert, T. Shirk, W.B. White, and Rustum Roy: *Mater. Res. Bull.*, 1968, vol. 3 (8), pp. 671–76.
23. H. Makram, L. Touron, and J. Lorries: *J. Cryst. Growth*, 1972, vol. 13, pp. 585–87.
24. E. Selcuk: *Ironmak Steelmak*, 1977, vol. 4 (2), pp. 116–18.
25. T. Katsura, K. Kitayama, T. Sugihara, and N. Kimizuka: *Bull. Chem. Soc. Jpn.*, 1975, vol. 48 (6), pp. 1809–11.
26. J.W. Nielsen and S.L. Blank: *J. Cryst. Growth*, 1972, vol. 13, pp. 702–05.
27. T. Katsura, T. Sekine, K. Kitayama, T. Sugihara N. Kimizuka: *J. Solid State Chem.*, 1978, vol. 23 (1), pp. 43–57.
28. S.C. Parida, S. Dash, Z. Singh, R. Prasad, K.T. Jacob, and V. Venugopal: *J. Solid State Chem.*, 2002, vol. 164 (1), pp. 34–41.
29. Y.P. Vorobev, A.A. Iovlev, and A.N. Men: *Russ. J. Phys. Chem.*, 1979, vol. 53 (6), pp. 800–03.